COBEM 2021 26th International Congress of Mechanical Engineering
November 22-26, 2021, Virtual Congress, Brazil

COB-2021- 0102
ANALYSIS OF AIRFOIL MOTION WITH TWO DEGREES OF FREEDOM: STUDY OF THE INITIAL VELOCITY OF THE FLUTTER BASED ON STEADY AND QUASI-STEADY ANALYSIS

Gabriel Vicentin Pereira Lapa
Alfredo Gay Neto
Guilherme Rosa Franzini
Polytechnic School at University of São Paulo. 380 Professor Luciano Gualberto Avenue, São Paulo, SP, Brazil.
gabriel.lapa@usp.br
alfredo.gay@usp.br
gfranzini@usp.br

Abstract. *Flutter instability of an airfoil is characterized by coupling between two vibration modes, initially with close natural frequencies. When changing the free-stream velocity, the associated natural frequencies with such modes are changed. Therefore, depending on this velocity, the motion behaves with growing amplitude and, in practice, it represents the disruption of the airfoil structure. This paper aims to study the conditions for this growing-amplitude motion as well as to study the associated wind speed as a system parameter for which flutter takes place. The study is split into two parts: the first one is based on an analysis of the coupling of the natural frequency modes due to the incidence of the wind, thus the beginning of the flutter effect. An alternative way for finding the wind speed associated with flutter is via the Lyapunov's indirect method, considering the steady and quasi-steady aerodynamic theories. In the second part, a numerical time-integration simulation for an airfoil model was carried out considering steady and quasi-steady theories. The results were compared with other tools, with good agreement. Several analyzes were made for different wind speeds. All of them presented results coincident with Lyapunov's indirect method for their respective aerodynamics theories. The lag between the displacement and angular movement was 180º in all aerodynamics theories.*

Keywords: *flutter, Lyapunov's method, steady and quasi-steady theories.*

1. INTRODUCTION

The first flutter report was in 1903 with a monoplane built by Professor Samuel Langley (Blevins, 2001). Since then, several cases of flutter have occurred. A well-known case in civil engineering was the Tacoma bridge in 1940. The flutter effect is generated by dynamic instability and is associated with the interaction between aerodynamics, elasticity, and inertial forces (Hodges and Pierce, 2002). The flutter causes an increase in the amplitude of vertical and torsional vibration generated by the wind, which can lead to the disruption of the structure due to the coupling between natural frequencies (Chen *et al.*, 2018). The occurrence of flutter is influenced by various parameters, such as the relative position of aerodynamic center, mass center, elastic center, and bending and torsional stiffness of airfoil (Chen *et al.*, 2021).

Several models define the speed of the wind that initiates the flutter, among them, computational fluid dynamics. However, due to the high computational cost, researchers have studied the analysis of two-dimensional simplified airfoil models to predict the flutter onset (Li and Caracoglia, 2019).

This paper aims at two main objectives, the first one is to make an onset velocity analysis of the flutter using Lyapunov's indirect method. The second objective is to implement an analytical time-domain model and compare it with another methodology, based on a numerical implementation of a geometrically-exact rigid body motion. An analysis of the velocity of the beginning of the flutter was also elaborated for analytical, steady and quasi-steady methods, and finally, a study of lag phase between vertical and angular was developed.

2. THEORETICAL BACKGROUND

2.1 Classical Flutter

Figure 1 shows a typical section of an airfoil with two degrees of freedom. The lift force F_L, drag force F_D and the pitching moment F_θ are the applied loadings in the aerodynamic center, located at a quarter chord back from the leading edge. F_L' and F_θ' are the loadings translated to the elastic center. The elastic center can also be called as the shear center, center of flexure, or center of twist; it is a point where applying a transversal force, no torsion in the airfoil takes place. c is the chord of airfoil, θ is the angle of attack, that is, it is the angle between the airfoil chord and the wind. a is the distance

between the aerodynamic center and the elastic center, C.G. the center of gravity, S_x/m the distance between the elastic center and the C.G., m the mass per span S_x the first moment of area, c the chord length, and U the wind speed (Blevins, 2001).

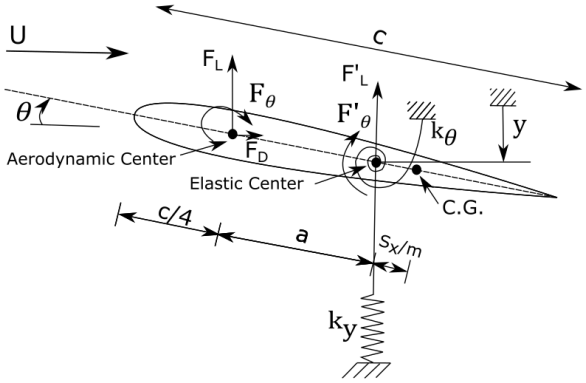

Figure 1 - Airfoil section supported by vertical and torsional strings.

The velocity of the airfoil can influence the aerodynamic loadings because the "perspective" angle of attack will be not just θ. Given a wind with parallel direction to the chord of an airfoil ($\theta = 0$) that has a vertical speed ($\dot{y}$) as illustrated in Figure 2a, the relative velocity of fluid will not be parallel. It will have a norm $|U_{rel}|$ and a γ angle with respect to U given by Eq. (1) for small angles. When the velocity is not being considered to calculate aerodynamics loadings the theory is called steady theory.

$$\varphi = \arctan\left(\frac{\dot{y}}{U}\right) \approx \frac{\dot{y}}{U}, \tag{1}$$

For the case that the airfoil is not parallel to the wind (Dowell, 2015):

$$\alpha = \theta + \varphi = \theta + \frac{\dot{y}}{U}, \tag{2}$$

where α is the instantaneous angle of attack.

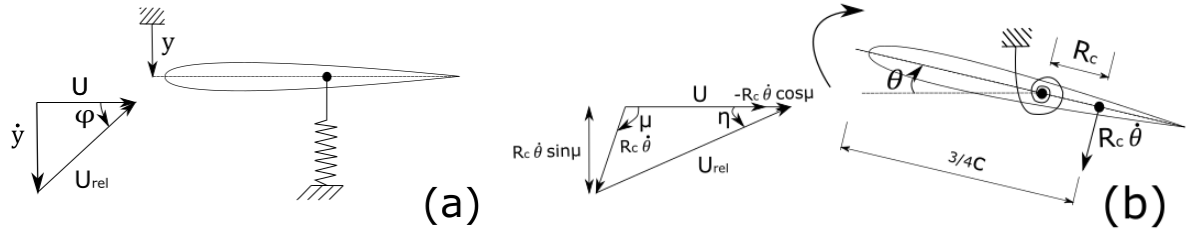

Figure 2 - Effect of airfoil vertical (a) and rotation (b) velocity from the instantaneous angle of attack.

The rotation velocity of airfoil ($\dot{\theta}$) also influences the instant angle of attack, but when the airfoil rotates, the relative velocity is different at each point. So, considering a distant reference point R_C from elastic center, that represents all points of the airfoil, (Fung, 1969) indicates that this point stays at ¾ of the chord from the leading edge as Figure 2b shows. So, the angle η will be:

$$\eta = \arctan\left(\frac{R_c\dot{\theta}sin\mu}{U - R_c\dot{\theta}cos\mu}\right), \tag{3}$$

considering small angles, β can approximate to 90º, therefore:

$$\eta \approx \frac{R_c\dot{\theta}}{U}, \tag{4}$$

so, the instantaneous angle of attack will be:

$$\alpha = \theta + \gamma + \eta = \theta + \frac{\dot{y}}{U} + \frac{R_c\dot{\theta}}{U}, \tag{5}$$

In this paper, when Eq. (2) is taken into account for the calculation of aerodynamic loadings, it is called quasi-steady theory 1 but when the Eq. (5) is considered, it is called quasi-steady theory 2

Physically the quasi-steady hypothesis means that the vortex-shedding frequency is much higher than the natural frequency of the structure. Therefore, the phenomenon of VIV (vortex-induced vibrations) does not become relevant (Franzini, 2019). (Blevins, 2001) indicates that for quasi-steady analysis the reduced velocity must be higher than 20, i. e.:

$$\frac{U}{f_n c} > 20, \tag{6}$$

where f_n is the natural frequency of vibration.

The loadings in the aerodynamic center are given by:

$$F_L = 0.5\rho U_{rel}^2 c C_L, \tag{7}$$

$$F_D = 0.5\rho U_{rel}^2 c C_D, \tag{8}$$

$$F_\theta = 0.5\rho U_{rel}^2 c^2 C_\theta, \tag{9}$$

where ρ is the air specific mass, C_L, C_D and C_θ are lift, drag, and moment coefficients. Their orders of magnitudes for small angle are: $C_L = 2\pi \sin\alpha$, $C_D = 0.01$, and $C_M = 0.01$. Therefore, when transferring them from the aerodynamic center to the elastic center, a moment is caused due the F_L by the offset a. This moment is much larger than F_θ, so, the force F'_θ can be written as being: $F'_\theta \approx aF_L$. F_D also generates a moment, but due to the small value of C_D, it was neglected. Thus, considering small angles of attack F'_L is equals to F_L.

The equation of motion, without considering damping, is given by the Eqs. (10) and (11).

$$m\ddot{y} + S_x\ddot{\theta} + k_y y = F_L, \tag{10}$$

$$S_x\ddot{y} + J_\theta\ddot{\theta} + k_\theta\theta = aF_L, \tag{11}$$

It is possible to expand the lift force in Taylor's series, resulting in:

$$F_L = -0.5\rho U_{rel}^2 c\left[C_L|_{\alpha=0} + \frac{\partial C_L}{\partial\alpha}|_{\alpha=0} + O(\alpha^2)\right], \tag{12}$$

For symmetric airfoil $C_L|_{\alpha=0}$ is zero. And its advantage is that it deals with a constant value ($\frac{\partial C_L}{\partial\alpha}$) depending on the variable θ instead of variable C_L . Thereby the Eqs. (10) and (11), can be written as:

$$m\ddot{y} + S_x\ddot{\theta} + k_y y = -0.5\rho U_{rel}^2 c\left(\frac{\partial C_L}{\partial\alpha}\right)\alpha, \tag{13}$$

$$S_x\ddot{y} + J_\theta\ddot{\theta} + k_\theta\theta = 0.5\rho U_{rel}^2 ca\left(\frac{\partial C_L}{\partial\alpha}\right)\alpha, \tag{14}$$

In a steady analysis, the angle of attack (θ) is equal to the torsion angle (α) and $U_{rel} = U$.

The solution of the system can be assumed by:

$$y = A_y e^{\lambda t}, \tag{15}$$

$$\theta = A_\theta e^{\lambda t}, \tag{16}$$

Here, t is time and A_y, A_θ and λ are constants. Using the Eqs. (15) and (16) into Eqs. (13) and (14), and organizing in matrix form, we have:

$$\begin{bmatrix} m\lambda^2 + k_y & S_x\lambda^2 + \frac{1}{2}\rho U^2 c\left(\frac{\partial C_L}{\partial \alpha}\right) \\ S_x\lambda^2 & J_\theta\lambda^2 + k_\theta - \frac{1}{2}\rho U^2 ca\left(\frac{\partial C_L}{\partial \alpha}\right) \end{bmatrix} \begin{pmatrix} A_y \\ A_\theta \end{pmatrix} = 0, \tag{17}$$

For Eq. (17) there is a trivial solution where $A_y = A_\theta = 0$, but in this case there is no motion. The other solution is found by making the matrix determinant in brackets equal to zero, so Eq. (18) is achieved.

$$C_0\lambda^4 + C_2\lambda^2 + C_4 = 0, \tag{18}$$

Its coefficients are given by:

$$C_0 = mJ_\theta - S_x^2,\ C_2 = m\left[k_\theta - \tfrac{1}{2}\rho U^2 ca\left(\tfrac{\partial C_L}{\partial \alpha}\right)\right] + k_y J_\theta - \tfrac{1}{2}\rho U^2 c\left(\tfrac{\partial C_L}{\partial \alpha}\right) S_x,\ C_4 = k_y\left[k_\theta - \tfrac{1}{2}\rho U^2 ca\left(\tfrac{\partial C_L}{\partial \alpha}\right)\right]. \tag{19}$$

Therefore, the values of λ are obtained by:

$$\lambda = \pm\left(\frac{\left[-C_2 \pm (C_2^2 - 4C_0C_4)^{1/2}\right]}{2C_0}\right)^{1/2}, \tag{20}$$

Normally the roots of Eq. (20) are complex numbers and their imaginary part corresponds to the natural frequencies of the structure. If λ has all four roots non-positive real parts, a small perturbation will vanish in time and the equilibrium point will be stable. If at least one of them has a positive real part, the motion will increase in time and the solution will be unstable. (Pines, 1958) solved the Eq. (20) to find the velocity that onset of flutter ($U_{flutter}$), i. e., $\lambda = 0$, leading to:

$$0.5\rho U_{flutter}^2 = \frac{-E \pm (E^2 - 4DF)^{0.5}}{2D}, \tag{21}$$

where:

$$D = \left((ma + S_x)c\frac{\partial C_L}{\partial \alpha}\right)^2, \tag{22}$$

$$F = \left(mk_\theta + k_y J_\theta\right)^2 - 4(mJ_\theta - S_x^2)k_y k_\theta, \tag{23}$$

$$E = \left[-2(ma + S_x)\left(mk_\theta + k_y J_\theta\right) + 4(mJ_\theta - S_x^2)ak_y\right]c\frac{\partial C_L}{\partial \alpha}, \tag{24}$$

Eq. (21) has two solutions, the flutter will occur if at least one of them is positive. If both are positive, the velocity that onset of flutter will be the smaller of them. In this paper, this method will be called “Pines’ method”.

Until now, the damping is not considered. Damping occurs due to energy dissipation during motion. Three phenomena generate this effect: fluid damping caused by the viscous dissipation, internal material damping due to yielding, heating, among others, and finally structural damping as a result of friction, impact, and others. The most common model for the damping force in structures is the ideal linear viscous damper. For the case of the airfoil with two degrees of freedom the damping forces are given by:

$$F_{dy} = 2m\zeta\omega_n\dot{y}, \tag{25}$$

$$F_{d\theta} = 2J_\theta\zeta_\theta\dot{\theta}, \tag{26}$$

where F_{dy} and $F_{d\theta}$ are the damping forces in the vertical and rotational directions, m the mass, ω_n the natural frequency, the ζ_y and ζ_θ are, respectively, the plunge and torsion damping factors, and ω_y is uncoupled natural frequency given by $\omega_y = \sqrt{k_y/m}$. This damping is considered only in the second part of this paper, considering $\zeta_y = 0.01$ and $\zeta_\theta = 0.01$.

In the case of quasi-steady 2, (Fung, 1969) through the vortex sheet, concluded that there is a damping proportional to the angular velocity relative to the pitching motion. This is caused by the Coriolis acceleration of fluid particles

(Haddadpour and Firouz-Abadi, 2006). Table 1 summarizes aerodynamic loadings used for the steady, quasi-steady 1, and quasi-steady 2 theories.

Table 1. Aerodynamic loadings used in the steady, quasi-steady 1, and quasi-steady 2 theories.

Theory	Aerodynamic loadings
Steady	$F_y' = -0.5\rho U^2 c\left(\frac{\partial C_L}{\partial \alpha}\right)\theta,$ $F_\theta' = 0.5\rho U^2 ca\left(\frac{\partial C_L}{\partial \alpha}\right)\theta$
Quasi-steady 1	$F_y' = -0.5\rho U_{rel}^2 c\left(\frac{\partial C_L}{\partial \alpha}\right)\left(\theta + \frac{\dot{y}}{U}\right),$ $F_\theta' = 0.5\rho U_{rel}^2 ca\left(\frac{\partial C_L}{\partial \alpha}\right)\left(\theta + \frac{\dot{y}}{U}\right)$
Quasi-steady 2	$F_y' = -0.5\rho U_{rel}^2 c\left(\frac{\partial C_L}{\partial \alpha}\right)\left(\theta + \frac{\dot{y}}{U} + \frac{R\dot{\theta}}{U}\right),$ $F_\theta' = 0.5\rho U_{rel}^2 ca\left(\frac{\partial C_L}{\partial \alpha}\right)\left(\theta + \frac{\dot{y}}{U} + \frac{R\dot{\theta}}{U}\right) - \frac{\pi\rho U c^3}{16}\dot{\theta}$

2.2 Lyapunov stability

A system is described by equations of motion with generalized displacements $q_i(t)$, where $i = 1,2,3,\dots,n$ and n is the degreed of freedom of the system. Transforming its equations in the first order differential by introducing new variables $Y_1, Y_2, \dots, Y_{2n}$ such that $Y_{2i-1} = q_i$ and $Y_{2t} = \dot{q}_i$ one reached:

$$\dot{\boldsymbol{Y}} = \boldsymbol{g}(\boldsymbol{Y}). \tag{27}$$

The phase space is defined as the 2n-dimensional space of variables $Y_1, \dots, Y_{2n}$. Figure 3 illustrates the meaning of Lyapunov stability. $\boldsymbol{\delta Y^0}$ as a small perturbation in $t = 0$ in region delimited by $\delta(\varepsilon)$ with center in the undisturbed solution $\boldsymbol{Y^0}$ that stays at the origin of the phase space. The equilibrium point will be stable only if the solution is within ε for every instant of t and unstable if the solution is larger than ε (Savi, 2017) (Bazent and Cedolin, 2010) (Yang e*t al.*, 2019).

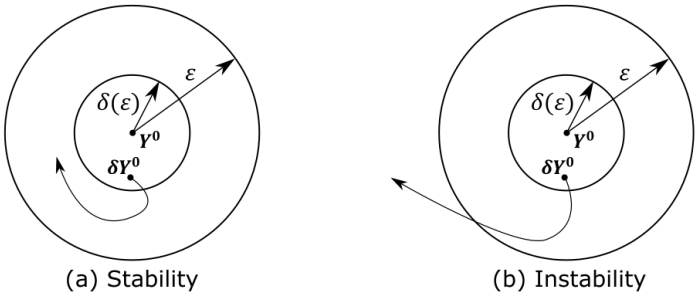

Figure 3. Solution trajectory: (a) Stability (b) Instability.

Adding $\boldsymbol{\delta Y^0}$ in the equilibrium point, one arrives to:

$$\boldsymbol{Y} = \boldsymbol{Y^0} + \boldsymbol{\delta Y}, \tag{28}$$

deriving:

$$\dot{\boldsymbol{Y}} = \dot{\boldsymbol{Y}}^{\boldsymbol{0}} + \boldsymbol{\delta \dot{Y}}, \tag{29}$$

substituting in Eq. (27) it is found that:

$$\boldsymbol{\delta \dot{Y}} = \boldsymbol{f}(\boldsymbol{\delta Y}) = \boldsymbol{A \delta Y} + \boldsymbol{N}(\boldsymbol{\delta Y}), \tag{30}$$

where $(\boldsymbol{A\delta Y})$ is the linear part and $(\boldsymbol{N}(\boldsymbol{\delta Y}))$ nonlinear part. In this study, the equations of motion are linear, so the non-linear part is not being considered. The matrix $\boldsymbol{A}$ is the partial derived of $\boldsymbol{f}$ with respect to $\boldsymbol{Y}$ calculated in the solution undisturbed:

$$\boldsymbol{A} = \left.\frac{\partial \boldsymbol{f}}{\partial \boldsymbol{Y}}\right|_{\mathbf{0}}, \tag{31}$$

The general solution is:

$$\boldsymbol{\delta Y} = \boldsymbol{\delta Y^{0}} e^{\lambda t}. \tag{32}$$

Substituting Eq. (32) into Eq. (30) the solution of the system is given by the eigenvalue problem. If the solution has any positive real numbers, the equilibrium point is Lyapunov-unstable.

3. METHODOLOGY

3.1 Part I

The imaginary parts of the roots of Eq. (20) provide the natural frequencies. So, by varying the wind speed it is possible to observe the variations of these frequencies. In this way, it is possible to detect the initial speed of the flutter.

Another way is the Lyapunov's indirect method. Equations (13) and (14) were transformed in the first order differential equations. Considering Eq. (30) one obtains:

$$\boldsymbol{B\dot{\delta q}} = \boldsymbol{A\delta q}, \tag{33}$$

where:

$$\boldsymbol{B} = \begin{bmatrix} 1 & 0 & 0 & 0 \\ 0 & 1 & 0 & \frac{S_x}{m} \\ 0 & 0 & 1 & 0 \\ 0 & \frac{S_x}{J_\theta} & 0 & 1 \end{bmatrix}, \ \boldsymbol{\delta \dot{q}} = \begin{Bmatrix} \delta \dot{q}_1 \\ \delta \dot{q}_2 \\ \delta \dot{q}_3 \\ \delta \dot{q}_4 \end{Bmatrix}, \tag{34}$$

$$\boldsymbol{A} = \begin{bmatrix} 0 & 1 & 0 & 0 \\ -\frac{k_y}{m} & 0 & \frac{1}{2m}\rho U^2 c\left(\frac{\partial C_L}{\partial \alpha}\right) & 0 \\ 0 & 0 & 0 & 1 \\ 0 & 0 & -\frac{k_\theta}{J_\theta} + \frac{1}{2}\rho U^2 ca\left(\frac{\partial C_L}{\partial \alpha}\right) & 0 \end{bmatrix}, \tag{35}$$

$$\boldsymbol{\delta q} = \begin{Bmatrix} \delta q_1 \\ \delta q_2 \\ \delta q_3 \\ \delta q_4 \end{Bmatrix}, \tag{36}$$

The matrix $\boldsymbol{B}$ is generated due to coupling given by S_x. Multiplying both sides of Eq. (33) by $\boldsymbol{B^{-1}}$:

$$\boldsymbol{\dot{\delta q}} = \boldsymbol{B^{-1}A\delta q}. \tag{37}$$

The instability of the system occurs when some eigenvalue of the result in Eq. (37) has a positive real part. For the quasi-steady cases, the procedure is the same, just considering the aerodynamic loadings in Table 1.

In this first part, it was considered the wing rig section of Ryan NYP. Its characteristics are (Blevins, 2001):

- chord (c): 2.13 *m*;
- slope of lift coefficient $\left(\frac{\partial C_L}{\partial \alpha}\right)$: 4.81;
- total mass per unit span (*m*): 14.4 *kg/m*;
- distance aerodynamic center forward of elas. Center (*a*): 0.0254 *m*;
- distance C.G aft elastic center (S_x/m): 0.297 *m*;
- polar mass moment of inertia per unit span (J_θ): 4.52 *kg/m²*;
- translational stiffness per unit span (k_y): 7060 *N/m*;
- torsional stiffness per unit span (k_θ): 2280 *Nm/rad*;

One meter in the span of the airfoil, air density 1.2 *kg/m³*, and elastic support were considered for the analysis.

3.2 Part II

In this part, simulations of airfoil motion were done in Giraffe software and Julia language (Bezanson *et al.*, 2017) using a one-meter profile. In the implementation developed in Julia language, it was used the Runge-Kutta 4th order method to numerically integrate the equations of motion given by Eq. (10), Eq. (11), and Table 1. Here, this method will be called the analytical method.

In Giraffe simulations were used a rigid body profile with bending and torsional stiffness formed by two vertical and rotational springs in each end as Figure 4 illustrates. Its motions in x and z are fixed, as well as the rotations in y and z, so only the degrees of freedom in y and rotation in x remain. The geometrically-exact theory was used (Neto A. G., 2016). The Newmark's method was utilized for the numerical integration with its coefficients settled at $\beta = 0.3$ and $\gamma = 0.50$.

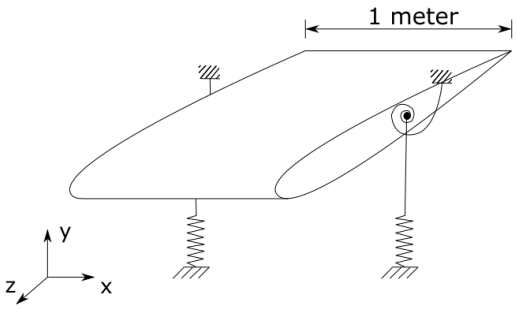

Figure 4. Schematic drawing of the model used in the Giraffe.

The aerodynamic loading hypotheses used in geometrically-exact motion analysis are slightly different from analytical. The drag force and pitching moment are taken into account, the coefficients C_L, C_D and C_θ were used directly from the curves of Figure 5 and by transferring the forces from the aerodynamic center to the elastic center the rotation of the airfoil was considered.

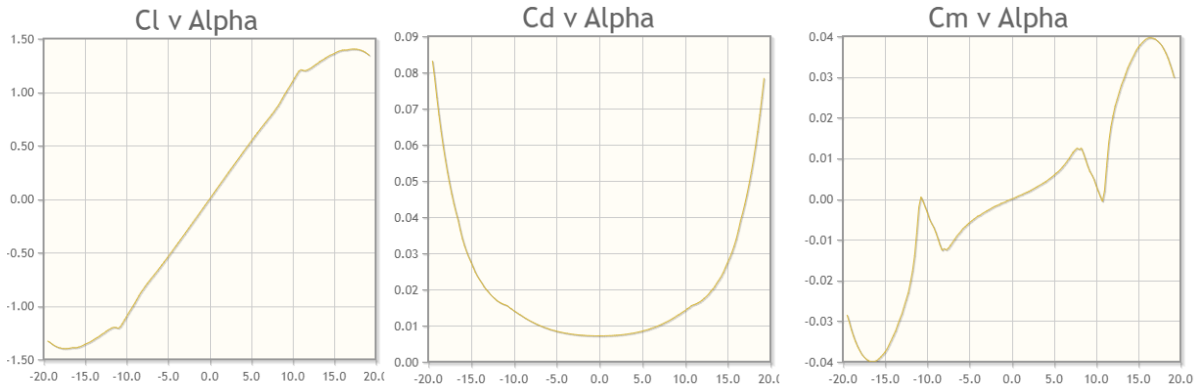

Figure 5. Lift, drag, and moment coefficients for the NACA 0018 *(Airfoil Tools)*.

The airfoil used was the NACA-0018 and its features were extracted by the WindTurbine software (Júnior *et al.*, 2018) (Júnior C. J., 2017). The characteristics used were:

- chord (c): 1 m;
- slope of lift coefficient $\left(\frac{\partial C_L}{\partial \alpha}\right)$: 2π;
- total mass per unit span (m): 106.0 *kg/m*;
- distance aerodynamic center forward of the elastic center (a): 0.0254 *m*;
- distance C.G aft elastic center (S_x/m): 0.2148 *m*;
- polar mass moment of inertia (J_θ): 14.66 *kg/m²*;
- translational stiffness per unit span (k_y): 203639 *N/m;*
- torsional stiffness per unit span (k_θ): 4525 *Nm/rad*;

For the analysis of the beginning of flutter, several simulations were elaborated where the motion of the NACA 0018 airfoil was verified in each one. This airfoil was also submitted to the onset of flutter analysis by Lyapunov's first method.

Finally, the lag angle between vertical and angular displacement was observed.

4. RESULTS

4.1 Part I

Through implementation in the Julia language (Bezanson *et al*., 2017), Eq. (20) for the airfoil described above was solved with wind speeds ranging from 0 to 25 m/s. Its results were divided into an imaginary part and a real part and are shown in Figure 6. Normally, in literature (Dowell, 2015), the speed and frequency are normalized. However, to facilitate the interpretation of the speed of the beginning of the flutter in the analysis, these quantities were not normalized.

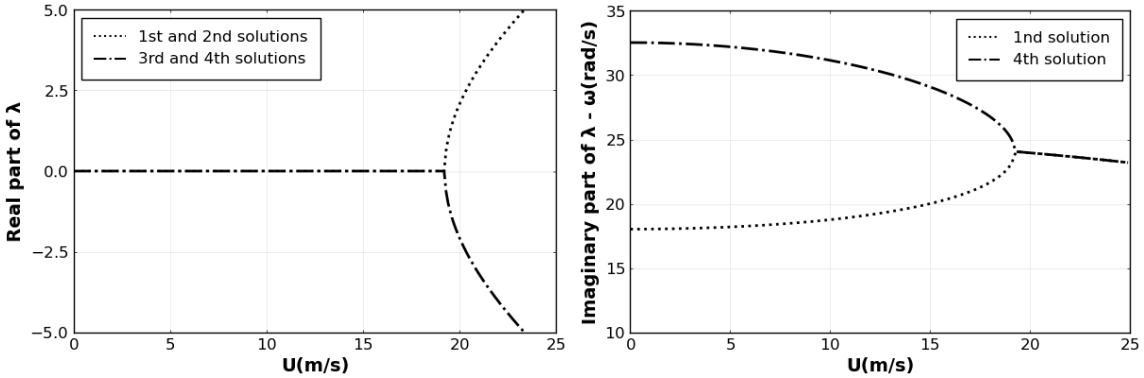

Figure 6- Real (left) and imaginary (right) part of four solutions of λ as function of wind speed.

As seen in the left chart of Figure 6, the real positive part starts with winds from around 19.2 m/s, indicating the onset of the flutter coinciding with the value in the literature (Blevins, 2001). The real part of the 1st and 2nd solutions are coincident, as well as the real part 3rd and 4th solutions. The right chart of Figure 6 shows only two solutions because the other two have the same module but with a negative sign. As one can be seen, the frequency coupling, also onset with 19.2m/s and its angular vibration frequency is 24.1 rad/s.

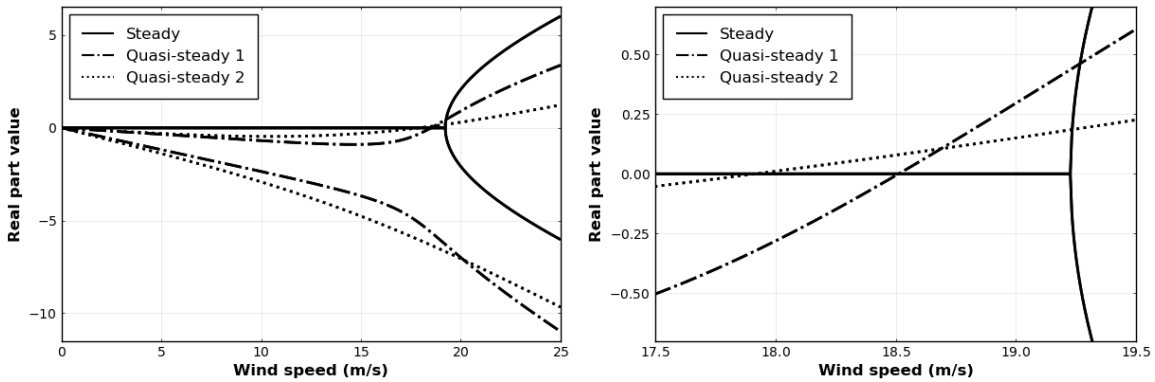

Figure 7 - Real part of the four eigenvalues for winds from zero to 25 m/s (left) and its zoom (right) by Lyapunov's indirect method.

Table 2- Flutter onset speed by Lyapunov's indirect method for steady and quasi-steady theories for Ryan NYP.

Analysis	Flutter onset speed by Lyapunov's indirect method (m/s)
Steady	19.2
Quasi-steady 1	18.5
Quasi-steady 2	17.9

To evaluate flutter onset speed by Lyapunov's indirect method the eigenvalues from Eq. (37) were obtained by the Matlab software (MathWorks, 2015) as a function of wind speed, resulting in four. Plotting the real part of these equations for the steady and quasi-steady theories, one arrives in Figure 7. In the case of the steady theory, the four solutions have zero as real part until 19.2 m/s and then two of the solutions appear a positive real part and another two negative ones. In quasi-stationary theories, the solutions were also superimposed, but for any non-zero wind speed. Table 2 shows the flutter onset speed by Lyapunov's indirect method for steady, quasi-steady 1, and quasi-steady 2 theories.

4.2 Part II

Figure 8 shows the vertical and rotation displacements of the NACA 0018 airfoil by the analytical method and the geometrically-exact motion for steady aerodynamic theory. An initial vertical displacement of 2 cm and with a wind of 40 m/s were considered. As can be seen, there was good agreement between them. The modules of maximum vertical and rotation displacement, in this case, were 0.02 m and 2.95º. For the quasi-steady 1 and quasi-steady 2 theory, there was also good adherence for small rotations.

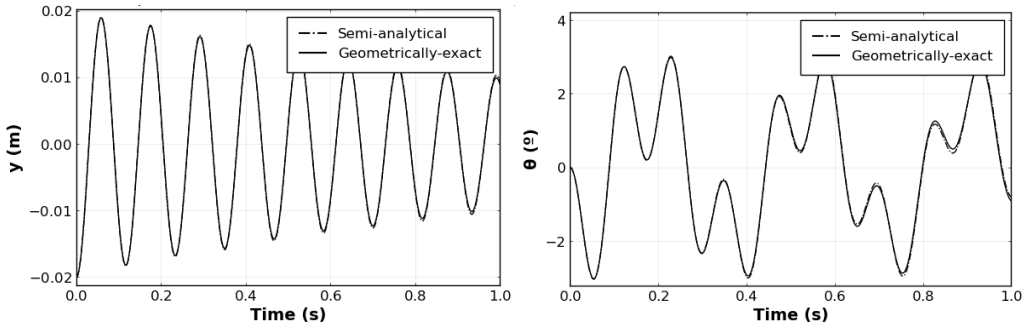

Figure 8. Comparison of vertical (left) and rotation (right) displacement of the airfoil between semi-analytical method and geometrically-exact motion.

Several time-domain analyzes were made for different wind speeds considering the NACA 0018 airfoil taking into account of the steady and quasi-steady theories. Observing the behavior of the airfoil, one can notice the initial flutter speed. Table 3 shows the results in comparison to Lyapunov's indirect method. As can be seen, the values were very close to each other. It is important to note that in all cases the reduced speeds were greater than 20.

Table 3. Comparison of the wind speeds associated with the onset of flutter for steady and quasi-steady analysis between Lyapunov's indirect method and semi-analytical method.

Aerodynamic theory	Flutter onset speed by Lyapunov's indirect method (m/s)	Flutter onset speed by the parametric study of semi-analytical method (m/s)
Steady	72.9	73.0
Quasi-steady 1	60.1	60.2
Quasi-steady 2	134.4	134.4

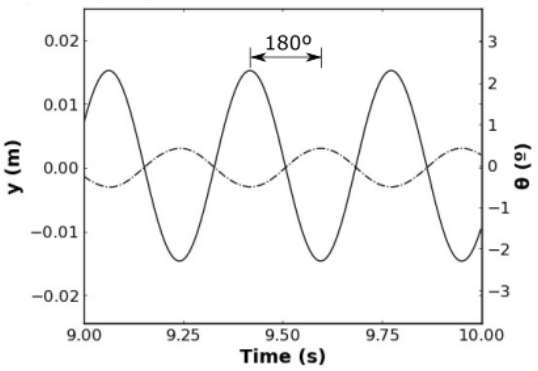

Figure 9. The vertical and torsional motion of a NACA 0018 airfoil using stead theory soon after the onset of flutter.

The motion after the flutter for steady theory is shown in Figure 9. Note that the vertical and rotational motions are sinusoidal with equal frequencies. In this way, it is possible to evaluate the lag phase between them. This lag is essential for extracts energy from the wind due to if either mode acting alone, the system would be stable (Abbas *et al*., 2017) (Blevins, 2001). For all three aerodynamic theories, the lag phase was around 180º.

5. CONCLUSION

In the first part of this paper, the coupling between vibration modes was shown due to the increased in wind speed. An alternative way to find the velocity that produces the onset of flutter by Lyapunov's indirect method was presented for

steady and quasi-steady aerodynamics theories. The obtained results coincided with Pines's method. In the second part, the implementation of the time-integration of the equations of motion of a rigid body airfoil with two degrees of freedom was done considering small rotations. Its results had a good agreement with a numerical implementation of a geometrically-exact rigid body motion where the drag force and the pitching moment were taken into account.

The equations of motion were integrated along time, generating plots for the airfoil displacement. By a parametric study, one can evaluate the wind speed associated with the onset of flutter instability. The results were remarkably close with Lyapunov's indirect method. The lag between the vertical and angular displacement for the steady and quasi-steady theories, for the case seen in this paper, were around 180º.

6. ACKNOWLEDGEMENTS

Author Gabriel Lapa wishes to thank Petrobras for his scholarship (agreement #5900.0112605.19.9). Authors Alfredo Neto and Guilherme Franzini acknowledge the National Council for Scientific and Technological Development (CNPq) under the grants 304680/2018-4 and 310595/2015-0.

REFERENCES

Abbas, T., Kavrakov, I., and Morgenthal, G., 2017. "Free Access Methods for flutter stability analysis of long-span bridges: a review". *Proceedings of the Institution of Civil Engineers - Bridge Engineering*, Vol. 170, No. 4, pp. 271-310.

Airfoil Tools. *NACA 0018 (naca0018-il) Xfoil prediction polar at RE=1,000,000 Ncrit=9.* http://airfoiltools.com/polar/details?polar=xf-naca0018-il-1000000. Accessed 7 June 2021,

Bazent, Z. P. and Cedolin, L., 2010. *Stability of Structures.* World Scientific Publishing Co. Pt.e Ltd, Singapure.

Bezanson, J., Edelman, A., Karpinski, S., and Shah, V. B., 2017. "Julia: A Fresh Approach to Numerical Computing". *SIAM review*, Vol. 59, No. 1, pp. 65-98.

Blevins, R. D., 2001. *Flow-Induced Vibration*. Krieger Publishing Company.

Chen, B., Hua, X., Zhang, Z., Nielsen, S. R., and Chen, Z., 2021. "Active flutter control of the wind turbines using double-pitched blades". *Renewable Energy*, Vol. 163, No. 1, pp. 2081-2097.

Chen, B., Zhang, Z., Hua, X., Nielsen, S. R., and Basu, B., 2018. "Enhancement of flutter stability in wind turbines with a new type of passive damper of torsional rotation of blades". *Journal of Wind Engineering & Industrial Aerodynamics*, Vol. 173, No. 1, pp. 171-179.

Dowell, E. H., 2015. *A Modern Course in Aeroelasticity.* Springer.

Franzini, G. R., 2019. *Tópicos de pesquisa em problemas de excitação paramétrica e de vibrações induzidas pelo escoamento* (in Portuguese). Habilitation theses, University of São Paulo, São Paulo, Brazil.

Fung, Y. C., 1969. *An introduction to the theory of Aeroelasticity.* Dover Publications.

Haddadpour, H. and Firouz-Abadi, R., 2006. "Evaluation of quasi-steady aerodynamic modeling for flutter prediction of aircraft wings in incompressible flow". *Thin-Walled Structures,* Vol. 44, No. 1, pp. 931-936.

Hodges, D. H. and Pierce, A. G., 2002. *Introduction to Structural Dynamics and Aeroelasticity.* Cambridge.

Júnior, C. J., 2017. *Modeling wind turbine blades by geometrically-exact beam and shell elements: A comparative approach*, Master's Thesis, University of São Paulo, São Paulo, Brazil.

Júnior, C. J., Cardozo, A. C., Júnior, V. M., and Neto, A. G., 2018. "Modeling wind turbine blades by geometrically-exact beam and shell elements: A comparative approach". *Engineering Structures*, Vol. 180, No. 1, pp. 357-378.

Li, S. and Caracoglia, L., 2019. "Surrogate Model Monte Carlo simulation for stochastic flutter analysis of wind turbine blades". *Journal of Wind Engineering & Industrial Aerodynamics*, Vol. 188, No. 1, pp. 43-60.

MathWorks, 2015. MATLAB (R2015a), version 8.5.0.197613. The MathWorks Inc, Natick, USA.

Neto, A. G., 2016. "Dynamics of Offshore Risers using a Geometrically-exact Beam Model with Hydrodynamic Loads and Contact with the Seabed". *Engineering. Structures*, Vol. 125, No. 1, pp. 438-454.

Neto, A. G.. *Giraffe Software (Generic Interface Readily Accessible for Finite Elements)*. Universidade de São Paulo. São Paulo.

Pines, S., 1958. "An Elementary Explanation of the Flutter Mechanism". *Proceedings National Specialists Meeting on Dynamics and Aeroelasticity*, pp. 52-58.

Savi, M. A., 2017. *Dinâmica Não-linear e Caos (in Portuguese).* e-papers, Rio de Janeiro.

Yang, L., Qiong, W., and Jianhua, Z., 2019. *Adaptive Sliding Mode Neural Network Control for Nonlinear Systems.* Academic Press, London, England.

7. RESPONSIBILITY NOTICE

The authors are the only responsible for the printed material included in this paper.